Chemical Science

ROYAL SOCIETY OF CHEMISTRY

EDGE ARTICLE

View Article Online
View Journal

Cite this: DOI: 10.1039/d6sc02121b

All publication charges for this article have been paid for by the Royal Society of Chemistry

Identifying the impact of chemical functional groups on ionic liquid conductivity

J. E. Umaña, N. A. Zawicki, Matthew A. Gebbie, Victor M. Zavala and Rose K. Cersonsky *

Ionic liquids are non-flammable, electrochemically stable electrolytes with promise as next-generation battery electrolytes. However, strong ion correlations and deviations from classical ion transport prevent the predictive design of application-specific ionic liquid electrolytes. While machine learning models can help address such limitations, standard cheminformatics tools are not well-suited to incorporate electrostatic interactions and thus do not account for the strong intermolecular interactions within ionic liquid materials. In this work, we present a molecular fragment representation that reflects charge-carrier resonance using SMARTS molecular substructure searching to explicitly capture the electrostatic contributions to conductivity of ionic liquid compounds. We find that this representation simplifies structure–conductivity relationships and improves predictive performance in low-data regimes. Additionally, we report how learned contributions of molecular structure impact ion transport and map the ionic liquid chemical design space using principal covariates regression to visualize the underlying structure–property relationships. We find that charge delocalization and anion flexibility are the most influential molecular features in improving ion transport in single-component ionic liquids. Further, we find that polar, alkyl, and fluorinated cation or anion functionalization decrease ion transport by introducing additional intermolecular interactions. Finally, many cation charge centers similarly enhance ion transport, suggesting that ionic liquid anions and ion functionalization are key for tuning intermolecular interactions and ion mobility. This work provides an interpretable approach for building structure–property relationships for currently available ionic liquid structures and opens new perspectives on how to design ionic liquids for desirable transport behavior. All data and models are shared as open-source code.

Received 13th March 2026
Accepted 26th May 2026

DOI: 10.1039/d6sc02121b

rsc.li/chemical-science

Introduction

As demands for large-scale renewable energy storage increase, ionic liquids have emerged as a promising electrolyte for use in electrochemical energy storage devices.[1] Ionic liquids are organic, electrochemically stable electrolytes which offer a wide variety of molecularly tunable behaviors for application-specific design.[2–4] Ionic liquids are composed entirely of ions yet remain liquid at room temperature due to poor molecular packing that inhibits crystal structure formation.[5] These materials have low vapor pressures and high stability due to strong electrostatic interactions. Ionic liquids can also reorganize in the presence of an electric field and display a favorably wide stable voltage-window.[6–8] All of these properties make ionic liquids desirable for electrochemical applications, particularly when device safety is a major consideration. Unfortunately, ionic liquids present a critical design challenge[2–4,9,10] – there are innumerable combinations of cations, anions, and functional groups[1,3] that make exploratory work combinatorically prohibitive. Furthermore, there is a large diversity of interactions between different cation–anion pairings, such that there exists strong deviations from overarching theories,[11] and data-driven approaches have struggled to generalize in this data-poor space.[9,12–14] For example, while polar functionalization typically increases the viscosity of a conventional uncharged liquid solvent, studies have found that cation ether functionalization in imidazolium bis(trifluoromethane)sulfonimide and pyrrolidinium bis(trifluoromethane)sulfonimide ionic liquids can instead decrease viscosity, despite the introduction of polar interactions that are not present in alkyl-functionalized analogues.[15,16]

To improve ionic liquid design as electrolytes, many studies have modeled ionic liquid conductivity using advanced machine learning and ionic liquid molecular descriptors.[9,12–14,17–27] While having been used successfully to predict electrolyte conductivity,[13,14,27,28] these machine learning models often utilize neural network and random forest regressions to correlate molecular summarizing statistics (molecular volume, partial charge, connectivity, *etc.*) to electrolyte properties of interest. Thus, the best performing neural network

Department of Chemical Engineering, University of Wisconsin–Madison, Madison, WI 53706, USA. E-mail: rose.cersonsky@wisc.edu

models provide limited insight into further ionic liquid design principles due to their high computational complexity. Many of the molecular descriptors employed in these models further complicate model interpretation as they do not provide actionable design insights, such as electronic states and polar surface area. For example, positive correlations between zero-order Randić's molecular connectivity indices and conductivity successfully identified by Dhakal and Shah using deep learning models and Shapley analysis accurately predict ionic liquid conductivity but do not provide sufficient guidelines for novel ionic liquid design.[28]

Our previous work has analyzed applications of classical transport models and machine learning models for predicting molar conductivity for ionic liquid design.[12,13] Notably, we found ionic liquids to deviate from hydrodynamic ion transport models and instead exhibit Arrhenius conductivity-temperature scaling consistent with ion hopping mechanisms. The energy barriers resulting from an Arrhenius model fit were within 15% of reported ion dissociation energies in literature and support a thermally-activated ion transport mechanism.[1,12] These findings agree with observed ion hopping transport mechanisms in ionic liquid simulations which strongly depend on electrostatic interactions and nanoscale assembly rather than bulk viscosity,[29–32] and our analysis is consistent with Vogel-Tamman-Fulcher models which model thermally-activated ion transport of broad distributions of activation energies in analogous polymeric and glassy materials.[1,33–35] We additionally explored the capabilities of machine learning methods to predict ionic liquid properties modeling using widely-available molecular structure representations.[12,13] Across machine learning models, we observed that electronic descriptors are consistently the most important molecular descriptors for predicting ionic liquid ion transport. These molecular descriptors likely proxy less accessible molecular information, such as ionic and intermolecular interactions.[12,13,25,28] Overall, we found that improving prediction of ionic liquid conductivity required new data representations that explicitly describe molecular interactions.

This work directly addresses this key technological need through fragment descriptors. Fragment descriptors are one-hot encodings that catalog the present functional groups within a system as a basis for predictive tasks. Here, we represent ionic liquid molecular structures using Simplified Molecular Input Line Entry System (SMILES) and define a minimal set of descriptors using SMILES arbitrary target specification (SMARTS) to represent 36 ionic liquid molecular fragments to model molecular structure contributions to room-temperature and temperature-dependent ionic molar conductivity. To train our model, we utilize a database of 182 ionic liquid structures and calculate molar conductivities using experimentally reported electrical conductivities and density measurements from the NIST ILThermo database.[36,37] We choose to model molar conductivity to remove the effects of ion concentration and compare ionic liquid motifs using equivalent conductivities. By using a molar/molecular basis, we isolate the effects of molecular structure on ion mobility similar to well-established mechanistic ion transport models such as the Stokes–Einstein equation and Walden plot analyses.[13,38,39] We further model molar conductivity at 298 K to identify the conductivity contribution of ionic liquid structures without the influence of temperature. To our knowledge, this study is the first in literature to model ionic liquid conductivity and ion mobility without convolving the effects associated with changes to temperature or ion concentration.

We define our substructure fragments using SMARTS according to electronic resonance and common ionic liquid functional groups and compare to an analogous 166 MACCS Keys for drug discovery as inputs to various regression methods.[40,41] SMARTS is a text-based molecular encoding used to specify molecular fragments and attributes in molecular structures by identifying the presence of specified molecular motifs.[42] SMARTS can identify patterns based on aromaticity, bond type, bond degree, connectivity, atom type, chirality, charge, and ring size. These patterns can then be used to discover structure–property correlations. For example, SMARTS were recently used to determine the contribution of molecular patterns to organic crystal binding energy.[43] We use only 2D molecular descriptors which are relevant to ionic liquid intermolecular interactions to simplify machine learning modeling and enable the development of structure–property relationships. Importantly, we explicitly distinguish the functionality of charge-carrying and neutral molecular fragments and define descriptors for electrostatic steric shielding in ionic liquids. To encode resonance and charge delocalization in our SMARTS fragment representation, all resonant structures for charge-carrying molecular fragments are specified in our SMARTS definitions. These definitions are included in the supplementary information in Table S4.

Overall, we contrast the performance of various machine learning techniques for modeling ionic liquid conductivity using SMARTS descriptors and mapping the ionic liquid chemical design space. We find that our molecular fragmentation results in simplified ionic liquid modeling, especially in low-data regimes. Notably, a Gaussian kernel support vector regression is used to identify the contributions of ionic liquid structural motifs to ionic conductivity at 298 K and at varied temperatures. We contrast our temperature-dependent model to our 298 K model to observe how motif contributions vary with increased temperatures. We find that anion identity and cation functionalization are the most influential aspects to determining ionic liquid conductivity, while most cation cores tend to contribute similarly to ion conduction in ionic liquids. In particular, asymmetric and charge delocalized anions paired with cations with weakly interacting functional groups exhibit the greatest enhancements in ion conduction compared to other ionic liquids, hence these features and may be opportune for tuning ionic liquid behavior. We anticipate that the approaches and results we describe can guide future studies into ionic liquid ion transport and provide design principles for studies into more complex ionic liquid mixtures.

Results & discussion

Ionic liquid molecular fragments were defined according to anion and cation charge cores and common ionic liquid

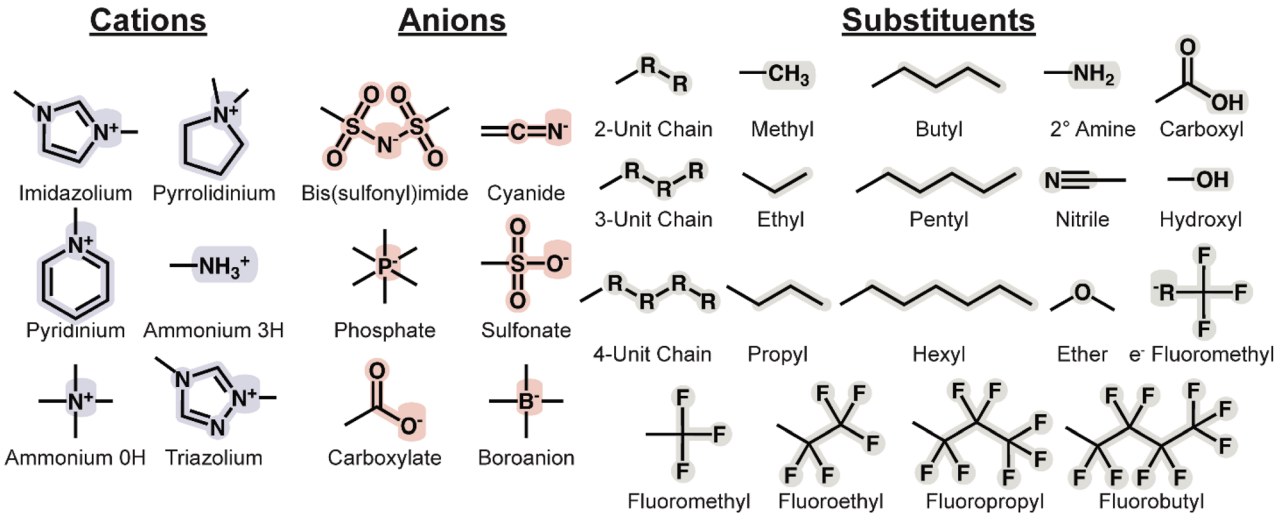

Fig. 1 Defined ionic liquid SMARTS keys. Cations and Anions are defined by charge localization, and all resonant structures are used in indexing ionic liquids in this study. Substituents are indexed separately for their presence in cation and anion molecular structures.

substituents. The ionic liquid molecular fragments we define are shown in Fig. 1 and SMARTS definitions for the corresponding structural fragments can be found in the supplementary information in Table S4. The presence of these structures in anion and cation molecular structures is indexed to produce ionic liquid representations used in all subsequent analysis. Ionic cores are defined by the location and resonance of ionic charges. Meanwhile, substituents are defined by common ionic liquid functionalization and are separately indexed for presence on either a cation or anion.

These structural fragments were selected for their prominence among ionic liquids analyzed in this study and down selected from a broader list of ionic liquid ion cores and functional groups. Structural fragments either over-represented (>179/182) or underrepresented (<4/182) in the reported dataset of ionic liquids with room-temperature conductivity were excluded from our SMARTS keys to limit overfitting and redundancy in our modeling. Notably, piperidinium cations were excluded from our fragments due to limited data at 298 K and could not be compared to other ionic liquid cations in this study.

Structural insights

We predict ionic liquid molar conductivities at 298 K and at all available temperatures using radial basis function (RBF) kernel ridge regression to model the contributions of ionic liquid structure to molar conductivity using interpretable, shallow methods. We also model molar conductivity using linear support vector machine regression, random forest regression, and neural network regression for comparison in following sections. 10-fold cross validation was applied in training the model and test performances are reported. We report RBF kernel ridge regression to perform the comparable to neural networks for our SMARTS keys representation at 298 K with an R^2 of 0.764 and MSE of 0.388 S cm^2 mol^{-1} compared to an R^2 of 0.820 and MSE of 0.340 S cm^2 mol^{-1} for our neural network regression. Similarly, at all available temperatures, an RBF Kernel ridge regression using our representation exhibits an R^2 of 0.838 and MSE of 0.778 S cm^2 mol^{-1} compared to an R^2 of 0.848 and MSE of 0.751 S cm^2 mol^{-1} for our neural network regression. While we cannot compare our room-temperature model predictions to literature due to limited prior successes in modeling ionic liquid conductivity at 298 K, our modeling at all temperatures is comparable to contemporary machine learning models yet with reduced model complexity and improved model interpretability.[12–14,18,19,27] The RBF kernel regression model test predictions are shown in Fig. 2 and further analysis of the model is discussed in this section. Model performance metrics for all models and a comparison to publicly available MACCS Keys are reported in Tables 1 and 2 and discussed in the corresponding section.

RBF kernel ridge regression fits the molecular fragments by learning the contributions of Gaussian-weighted similarity between an input fragment vector and those within the training set, as shown here:

$$\Lambda_i = \sum_j w_j e^{-\frac{\|x_i - x_j\|^2}{2\sigma}}$$

where Λ_i is the predicted molar conductivity, w_j are fit weights for each ionic liquid, σ is a user-defined model hyperparameter, x_i is the input structure represented as our SMARTS keys, and x_j are the structures of each other ionic liquid represented with SMARTS Keys. This allows greater flexibility for representing molecular fragment contributions to conductivity compared to linear regression as the model does not directly predict the influence of each molecular fragment. Rather, the contributions of the molecular fragments we define to conductivity are implicitly captured within the distribution of learned weights for structural similarity to ionic liquid structures containing a given structural fragment of interest. We then subsequently extracted weights for specific structural fragments by probing the model with bit-flip perturbations and are reported in Fig. 3.

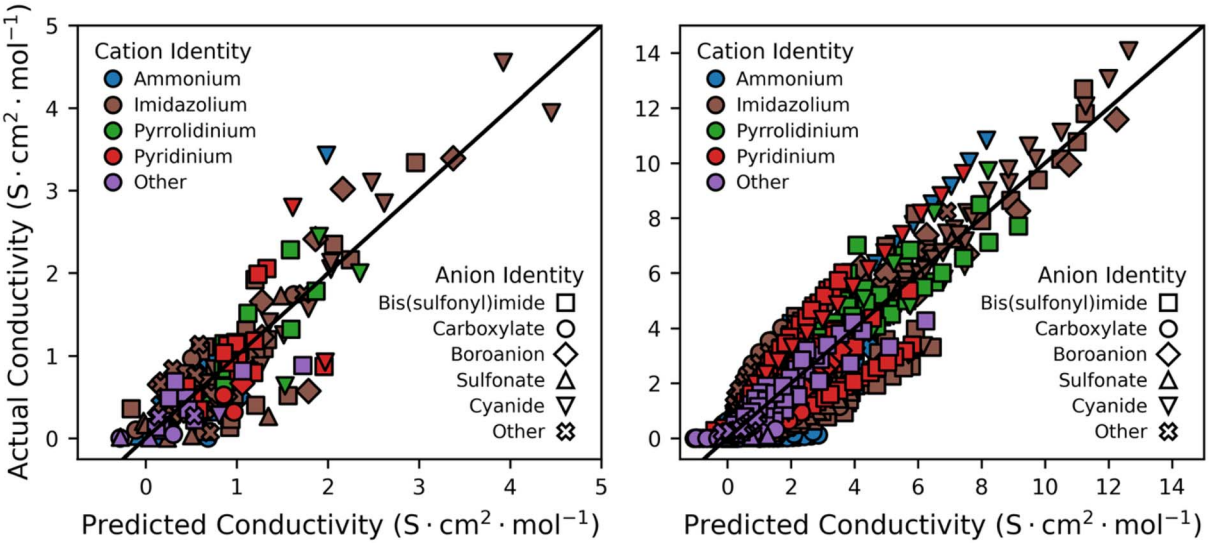

Fig. 2 RBF Kernel SVM parity plot colored by cations and shaped by anions for 298 K (left) and at all temperatures (right). We find that the most well-represented groups appropriately have the highest variability as these groups possess the highest variability in measured conductivity and are not being overfit by our modeling.

Table 1 Test set coefficients of determination (R^2) and root mean squared errors (RMSE) for linear ridge regression, RBF kernel regression, random forest regression, and multi-layer perceptron neural network regression models employed for conductivity at 298 K using the SMARTS representation we developed (SMARTS), MACCS Keys (MACCS), and a 36-dimension MACCS principal component representation (PCA MACCS)

Model	SMARTS R^2	SMARTS RMSE	MACCS R^2	MACCS RMSE	PCA MACCS R^2	PCA MACCS RMSE
Ridge regression	0.563	0.529	0.516	0.557	0.432	0.579
RBF kernel regression	0.764	0.388	0.733	0.414	0.690	0.445
Random forest regression	0.667	0.462	0.620	0.493	0.435	0.602
MLP neural network	0.820	0.340	0.830	0.330	0.678	0.454

Table 2 Test set coefficients of determination (R^2) and root mean squared errors (RMSE) for linear ridge regression, RBF kernel regression, random forest regression, and multi-layer perceptron neural network regression models employed for conductivity for all temperatures using the SMARTS representation we developed (SMARTS), MACCS Keys (MACCS), and a 36-dimension MACCS principal component representation (PCA MACCS)

Model	SMARTS R^2	SMARTS RMSE	MACCS R^2	MACCS RMSE	PCA MACCS R^2	PCA MACCS RMSE
Ridge regression	0.635	1.167	0.670	1.109	0.639	1.160
RBF kernel regression	0.838	0.778	0.863	0.715	0.838	0.777
Random forest regression	0.787	0.890	0.784	0.897	0.642	0.994
MLP neural network	0.848	0.751	0.888	0.647	0.863	0.715

Importantly, the improved performance of RBF kernel regression over linear regression indicates that the influences of molecular structure fragments cannot be linearly combined as independent, 0th order contributions to conductivity and is instead a complex combination of physical and chemical interactions. This supports findings that ion transport in ionic liquids is strongly influenced by emergent phenomena such as nanostructuring, ion aggregation, and correlated ion transport which can all potentially vary ion transport pathways.[3,15,16,29,44,45] For example, multiple studies report greater changes to nanoscale structuring in functionalized imidazolium cations than in functionalized pyrrolidinium cations despite being functionalized with identical chemical structures[16,46] suggesting that interactions between ionic liquid ion cores and functional groups are critical for describing ion coordination and are not independent contributions to ionic liquid chemical phenomena. Furthermore, the improved performance of the kernel regression implies that *similar chemistries exhibit similar nanostructuring*.

Further analyzing our regression modeling, we first note that some ionic liquids in our dataset exhibit large predictive errors near 0 S cm^2 mol^{-1} across all models and representations.

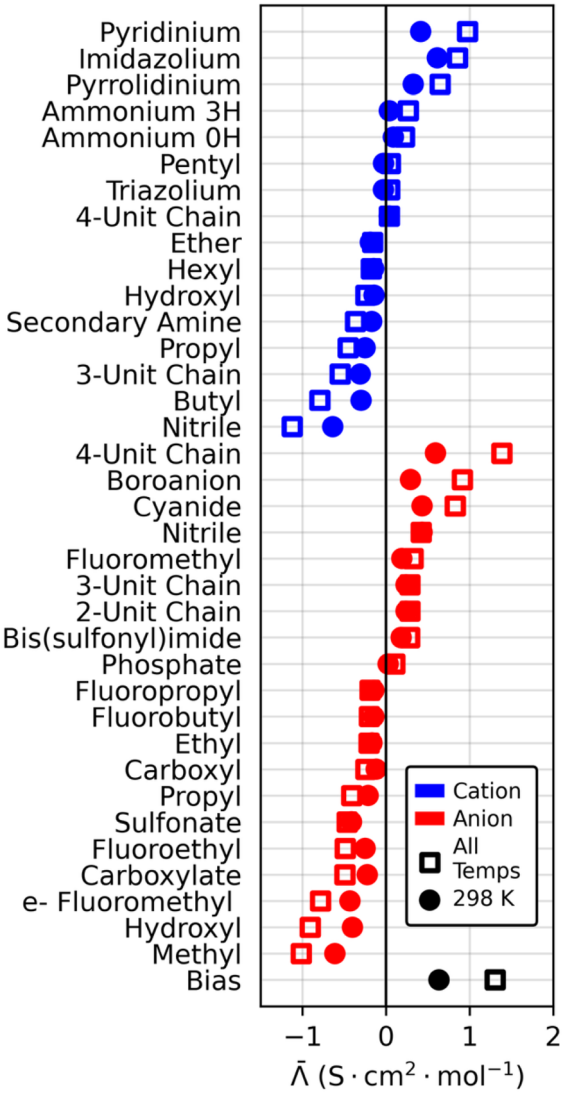

Fig. 3 RBF Kernel SVM model contributions at 298 K and at all temperature. These weights show the modeled contributions of ionic liquid molecular substructures to ionic liquid molar conductivity. Contributions for the conductivity model at 298 K and all temperatures are represented as filled in circles and empty squares, respectively. Cation substructures are shown on top in blue, anion substructures are below in red, and model bias is shown in black. We observe that aliphatic tails and anion identities have the largest contributions to ionic conductivity.

These predictions are visualized in Fig. 2 and in the SI in Fig. S5–S28. These ionic liquids are mostly comprised of protic ionic liquids with sulfonate and carboxylate anions and exhibit weak conductivity-temperature scaling which likely results from ion neutralization. Protic ionic liquids exist in an equilibrium of charged and neutral species in which neutralized ions drastically reduce conductivity and the degree of ionization.[55] Although, the extent of ion neutralization ranges widely and is affected by factors such as proton transfer and synthesis conditions.[38] For example, weak acids, such as amino acids used in the synthesis of 2-hydroxy-*N*,*N*,*N*-trimethylethanaminium L-serinate (present in this dataset), can result in low degrees of ionization.[38,47,48] The difficulties in modeling ion neutralization from molecular structure descriptors highlight opportune areas of study to improve ionic liquid computational descriptors and advance our understanding ionic liquid behavior.

While ionic liquids with varying degrees of ionization are a challenge for machine learning models in low-data regimes, removing these ionic liquids from our dataset does not significantly impact the accuracy or the learned molecular contributions of our models. Most protic ionic liquids ionic liquids are generally well predicted by our model as these behave similarly to the remaining ionic liquids in our dataset. However, we note that further complexities may arise for protic ionic liquids near the glass transition temperature and at high pressures, where Grotthus-type proton transport becomes non-negligible to ion conduction.[49] Overall, this domain of ionic liquid chemistry is a rich space for further investigation *via* molecular simulations, calculations, or experiments to refine theory and design.

Continuing the analysis of our RBF model, we can determine weights assigned to each functional group by bit-flip perturbation analysis. We pass synthetic one-hot encodings with single "bits flipped" to the fitted model to identify their contribution to the conductivity predictions. As shown in Fig. 3, we find that the ionic liquid anion cores span a significantly larger range of contributions to molar conductivity compared to cation cores. This is likely due to greater variability in ionic liquid anion structures.[1,2,12,32,47] We find that flexible and charge delocalized anions have the largest positive influence (enhancement) on conductivity as shown by the large weights for conformationally flexible 4-unit chains and delocalized bis(sulfonyl)imide and cyanide anions, respectively. Meanwhile, alkyl and polar functionalization on either ion have the largest negative contributions (suppression) on ionic conductivity. We also observe that fluoroalkyl functionalization beyond fluoromethyl functionalization is also predicted to reduce conductivity. These analyses suggests that the addition of strong intermolecular interactions and bulky fluoroalkyl groups reduce the ionic conductivity of ionic liquids.

We find that bis(sulfonyl)imide anions, cyanide anions, anions comprised of 4-unit aliphatic chains, and charge-delocalized cations (imidazolium and pyridinium) provide the greatest enhancing contributions to ionic liquid molar conductivity. This indicates that flexible, charge-delocalized ions provide the largest positive contributions to the ion mobility predicted by our model, agreeing with high conductivity observed in bis(trifluoromethylsulfonyl)imide, bis(fluorosulfonyl)imide, and cyanide-based anions.[1–3,50–53] High conductivity among ionic liquids containing charge-delocalized anions may result from weaker electrostatic interactions,[16,54] as weaker ion–ion interactions can reduce ion-pair aggregation and lower the energy barrier for ion conduction.[12,55,56] Meanwhile, flexible, asymmetric anions increase accessible molecular conformations[50,51,57] which alter the accessibility of certain ion transport pathways.[3,32,52] In contrast, phosphonate, sulfonate, and carboxylate anion cores significantly suppress ionic liquid conductivity compared to bis(sulfonyl)imide, cyanide, and boride anions. This suppression is attributed to stronger

intermolecular forces which also increase the viscosity of these ionic liquids and is potentially due to strong hydrogen bonding in phosphonate, sulfonate, and carboxylate species.[1,58]

Analyzing our learned cation contributions, we observe cationic cores are the most enhancing cation structural fragments for molar conductivity as charge delocalization and steric shielding are critical for ionic liquid fluidity.[59,60] Overall, imidazolium, pyridinium, pyrrolidinium, ammonium, and triazolium cation cores all provide relatively enhancing contributions to conductivity which suggests that these common cation cores demonstrate similar ionic interactions and may be limited in opportunities for modulating ionic liquid conductivity by solely changing cation ion cores.

Among the cation cores, we observe that aromatic cation cores with delocalized charges (imidazolium and pyridinium) exhibit a relatively higher contribution to conductivity than aliphatic cation cores with localized charges (ammonium and pyrrolidinium) in Fig. 3. Interestingly, pyridinium remains significantly less studied than imidazoliums in ionic liquid literature despite exhibiting similar enhancing effects on ion transport.[1] The origin of this enhanced contribution requires additional studies to deconvolute, however, as 2D molecular structure representations cannot isolate the effects of molecular geometry from charge delocalization for this dataset.

In particular, the SMARTS representations we developed does not account for conformational or steric effects which have been shown to affect transport in imidazolium-based and pyridinium-based ionic liquids.[61–63] For example, 1-ethyl-2-methylpyridinium bis(trifluoromethylsulfonyl)imide exhibits a molar conductivity of 0.87 S cm^2 mol^{-1} while 1-ethyl-4-methylpyridinium exhibits a molar conductivity of 2.06 S cm^2 mol^{-1} at 298 K but have identical SMARTS representations in our modeling. These steric effects have also been shown to arise in 1-ethyl-2,3-methylimidazolium tetrafluoroborate compared to 1-ethyl-3-methylimidazolium tetrafluoroborate where the methylation of the 2C site changes available anion transport pathways around the planar cation core and decreases ion mobility.[3,64] Similar effects likely exist for other imidazolium-based and pyridinium-based ionic liquids and would require additional data to model.

1,2,4-Triazoliums cation cores exhibit the lowest contribution to conductivity despite charge delocalization likely due to the higher Lewis acidity and stronger cation–anion interactions of the 1,2,4-triazolium cation core.[65,66] Other triazolium cores (1,3,4-triazolium and 1,2,3-triazolium) exhibit widely varied transport properties but are not present in this dataset.[3,66,67]

Analyzing ionic liquid functionalization, we find that increasing degrees of alkyl functionalization decreases conductivity for both cations and anions. This finding agrees with broader findings in the ionic liquids community, as increasingly long alkyl substituents on cations drive increasing degrees of nanoscale segregation into polar and apolar domains which correspondingly reduces ion mobility.[68–70] For cations, we find butyl functionalization contributes the largest decrease in conductivity for cation alkyl tails, aligning with studies that find butyl chains to be the shortest alkyl chains which form nano segregated regimes in imidazolium ionic liquids.[68–72] Meanwhile, anion methylation provides the largest decrease in conductivity for anion alkyl functional groups, although studies with alkyl functionalized anions are limited. Our dataset contains seven unique alkyl functionalized anions compromising of carboxylates, sulfonates, and phosphates anions and methyl, ethyl, propyl, and tetradecyl alkyl tails. While we find that anion alkyl functionalization decreases ion mobility, the mechanism for phenomena is an open question and recommended for future study.

Negative contributions from fluorinated functional groups are particularly notable, as these groups are often thought to improve transport dynamics in typical liquids.[53,59,73] Fluoroalkyl groups are highly stable and weakly-interacting chemical compounds that often reduce intermolecular interactions in typical liquids. Recently however, Brehm *et al.* found that fluoroalkyl substituents on ionic liquids self-assemble into fluorine-rich domains which may alter ion transport pathways.[68] Notably, these fluoroalkyl groups increase ionic liquid heterogeneity due to their disruption of polar and alkyl molecular domains which could complicate transport dynamics,[3,74] and provides further evidence suggesting that nanoscale phase segregations has a suppressing influence on ionic conductivity in ionic liquids and is recommended for further study. For example, Kang, *et al.* reported low ionization and conductivity in trihexyltetradecylphosphonium octofluoropentanoate; however, the transport dynamics of ions in fluoros domains remains an open question.[75]

In contrast, polar functional groups remove polar-apolar domain separation which can improve conformational dynamics and reduce barriers to ion transport in ionic liquids.[15,76] At the same time, polar groups also introduce new intermolecular interactions, such as hydrogen bonding and polar interactions which may locally stabilize ions, and reduce material fluidity compared to short alkyl-tail ionic liquids.[59,77] In agreement with many studies, we find that ionic liquids with polar groups exhibit higher conductivity and fluidity than alkyl-substituted analogs, *e.g.* 1-(2-methoxyethyl)-3-methyimidazolium bis(trifluoromethylsulfonyl)imide compared to 1-butyl-3-methylimidazolium bis(trifluoromethylsulfonyl)imide, as is shown by the ether and hydroxyl providing more positive contributions to conductivity than propyl and longer alkyl tails in Fig. 3.[78–80] However, polar-functionalized cation ionic liquids still remain overall less conductive than shorter-tail ionic liquids with fewer intermolecular interactions, *e.g.* 1-ethyl-3-methylimidazolium bis(trifluoromethylsulfonyl)imide,[81] as is depicted by the net-negative contributions to conductivity of ether and hydroxyl groups in Fig. 3.

Interestingly, we observe very similar trends for cation and anion functional groups, likely as functional groups perform a similar role in disrupting the dominant electrostatic interactions in ionic liquids. Thus, the largest differences in cation and anion conductivity contributions are exhibited by the ion cores, where dissimilar cations cores show similar effects to conductivity and dissimilar anion core identity can cause large variance in conductivity based on core identity.

Finally, we emphasize that these results are for the conductivity of pure ionic liquids only and contextualize that polar and fluorinated functionalization may be useful in improving the transport of other ionic species, such as redox ions. Previous studies show that polar functional groups may provide new transport pathways for Li in polymeric ionic liquids.[45,82–84] Our results can contextualize these findings by showing a general immobilization of ionic liquid cations upon the introduction of polar groups. The immobilization of ionic liquid cations or anions through polar, alkyl, or fluorinated functionalization could be leveraged to improve the transference of redox species and is appropriate for further study.[15,32,44,85–90]

Dimensionality reduction

Given the importance of nanostructuring in determining the behavior of ionic liquids, it is worthwhile to identify the convergence and divergences of chemical similarity as they relate to conductivity. We perform Principal covariates regression (PCovR) on our data set of molar conductivity at 298 K using our custom SMARTS fragment library and compare against a representation created using the widely applied MACCS Keys fragment library. PCovR is a weighted combination of principal components analysis (PCA) and linear regression and produces a linearly decomposed latent space (similar to PCA) oriented to correlate with a regression target.[91–93] Here, we visualize the linearly decomposed latent data spaces created by the SMARTS representation we developed and the MACCS Keys library with molar conductivity at 298 K as our regression target. Fig. 4 shows the 2-dimensional projection of our ionic liquid database overlaid with molar conductivity at 298 K and highlighted with representative ionic liquids. Weights for PCov 1 and PCov 2 are available in the supplementary information in Table S3.

We observe a strong trend between molar conductivity and the 2nd principal covariate (PCov) using our custom SMARTS representation; on the other hand, no significant trend is observed using the MACCS Keys representation. This observation indicates our approach of developing a custom SMARTS library can be used to more easily identify trends in low-data regimes and indicate chemistries of similar emergent transport phenomena. In particular, local regions within the SMARTS latent space with similar structure and conductivity delineate ionic liquids likely accessing similar ion transport mechanisms. Observing the resulting MACCS Keys latent space, we find the data to cluster largely by cation and anion identity without significant trends for conductivity or functionalization.

To further investigate trends between molecular similarity and ion conduction, we visualize the SMARTS PCovR latent space projection by highlighting points according to cation core identity, cation functionalization, and anion core identity in Fig. 5. Along PCov 2, we can identify structures which significantly correlate with molar conductivity; meanwhile, along PCov 1, we observe structural fragments which are structurally distinct but do not differentiate ionic liquid conductivity. We find that trends largely agree with our RBF kernel regression contributions and reaffirm that cation functionalization and anion core delocalization are the most influential structural motifs for tuning ion mobility ionic liquids. A visualization of the MACCS Keys PCovR latent space overlayed with cation identity, anion identity, and cation functionalization is available in the supplementary information in Fig. S3.

Cation core identities are distributed across both PCov 1 and PCov 2 values and do not exhibit strong trends with ionic liquid molar conductivity. This finding indicates that each cation core spans across the full range of molecular structure diversity within this data set and that each cation core can exhibit nearly the complete range of observed conductivities observed. In other words, cation core identity does not significantly distinguish the chemical diversity of ionic liquid structures nor the resulting ion transport behavior observed in this study. This conclusion agrees with the similar model weights observed for all imidazolium, pyrrolidinium, pyridinium, ammonium, and triazolium cation identities in kernel SVM modeling using SMARTS representations. We note that phosphonium cations are reported to result in high conductivity ionic liquids in literature, but are not widely studied enough to produce generalizable trends in this PCovR analysis.[3,30,31] Overall, ionic liquid ion transport behaviors do not significantly depend on the cation core and instead are influenced by their cation functionalization and anion pairings.

Cation functionalization exhibits a distinct trend in our data projection as cations functionalized with short alkyl tails are located at high PCov 2 values and low PCov 1 values while cations functionalized with long alkyl tails are located at low PCov 2 values and high PCov 1 values. These trends are best contextualized by also considering the differentiation of anion identity by PCov 1. Short alkyl tail cations are generally located at high PCov 2 values and exhibit greater conductivities for a given PCov 1 value and given anion core. This trend finds that conductivity generally decreases with increasing alkyl tail length and generalizes the commonly reported trend of decreased material fluidity with increasing tail length across cation and anion cores.[1,3,13,28] Polar functionalized cations are distributed across PCov 1 and PCov 2 but are located at lower PCov 2 values (and conductivities) than ethyl-functionalized cations for a given PCov 1 (and anion identity).

Anion core identities exhibit clustering in the PCovR data projection with bis(sulfonyl)imide and cyanide ionic liquids clustering at large PCov 1 values and sulfonate, carboxylate, boroanion, and other anion (halides, nitrates, phosphates, *etc.*) ionic liquids clustering at low PCov 1 values. Tetracyanoborate ionic liquids are also located at high PCov 1 values due to their cyano-group functionalization, and we note that these are labeled as Boroanions in Fig. 3. All anion groups exhibit a wide range of conductivities; however, cyanide and bis(sulfonyl) imide anions exhibit a greater maximum conductivity than sulfonate, carboxylate, boroanions without cyanide functionalization, and other anions in this dataset. Cyanide anions improve conductivity the greatest and are located at the highest Pcov 2 values. The broader range of observed conductivities for dicyanamide and bis(sulfonyl)imide anions is attributed to the asymmetric structure and conformational flexibility of these anions in simulations studies.[50,51,74] Carboxylate and sulfonate

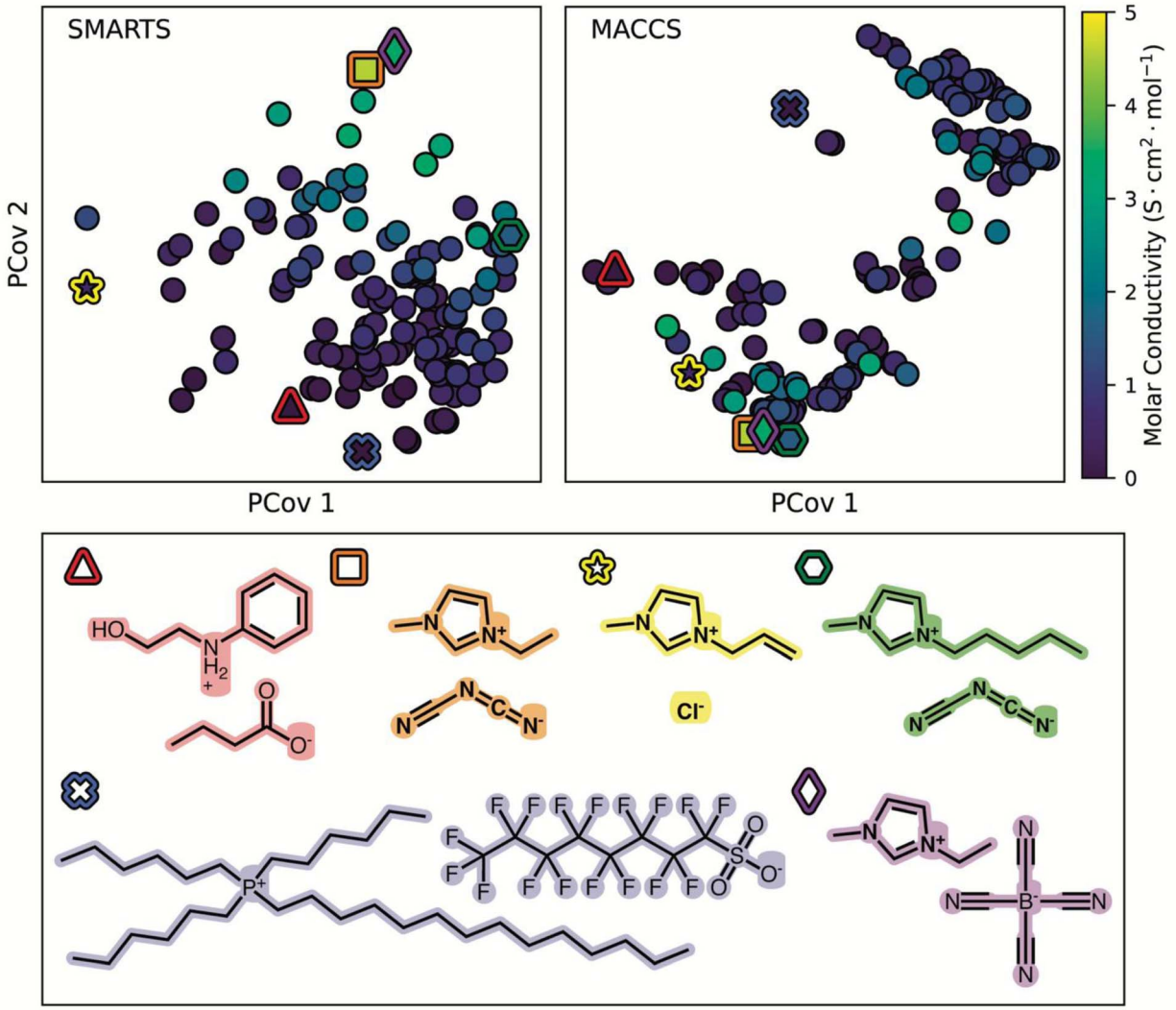

Fig. 4 A 2-dimensional data projection of 182 ionic liquids represented by our custom SMARTS fragmentation (Top Left) and MACCS Keys (Top Right) onto principal covariates overlaid with ionic liquid molar conductivity at 298 K. Representative molecular structures are shown (Bottom) by shape and color to illustrate the chemical space mapping. Using our custom fragment representation, conductivity is primarily captured in the 2nd principal covariate with highly conductivity ionic liquids located at high 2nd PCov values while the 1st PCov captures variations in ionic liquid structure which are largely irrelevant to conductivity. MACCS Keys, in contrast, do not produce a 2D projection which correlates with molar conductivity and gives large weights to cation similarity despite large differences in anion identity and molar conductivity.

anions exhibit lower conductivity as these anions can strongly hydrogen bond and have stronger intermolecular interactions.[3,94]

The most conductive ionic liquids are located at the highest PCov 2 values and consist almost entirely of cations functionalized with ethyl or propyl alkyl tails and cyanide, bis(sulfonyl) amide anions, or tetracyanoborate anions. Ethyl and propyl cation substituents interact weakly and do not form significant apolar regions in ionic liquid nanostructures.[68–72] Meanwhile, cyanide based and molecularly flexible fluorinated anions (such as cyanide, tetracyanoborate, and bis(sulfonyl)imide anions) have highly delocalized or shielded anion charges and exhibit high degrees of conformational flexibility in reported molecular dynamic simulations.[2,50,51,57,74] These similarities in molecular behavior amongst the highest conductivity ionic liquids suggest that weakly-interacting cation functionalization and low anion charge density may be a key combination high ion mobility in ionic liquids. In particular, this combination of molecular behaviors may result in similar material nanostructures and ion transport pathways which are conducive to high molar conductivities, and we recommend these ionic liquids for further investigations.

Regression model comparisons

In addition to the RBF kernel model, we created predictive conductivity models using linear ridge regression, random

forest regression, and multi-layer perceptron artificial neural network regression using the custom SMARTS representation, a MACCS Keys representation, and a MACCS Keys principal component latent space representation to compare the capabilities of molecular fragments for use in predictive modeling. We reduced the dimensions of the MACCS Keys representation to 36 dimensions using principal component analysis to match the dimensionality of our custom SMARTS representation. Shallow machine learning models created using our custom SMARTS representation perform better than models using MACCS keys at 298 K, while models using MACCS Keys perform slightly better when all temperatures are included. Reduced dimensionality MACCS Keys performed worse than either MACCS Keys or custom SMARTS representations in nearly all cases—further reinforcing the benefits of custom SMARTS fingerprint representations. For MACCS Keys and custom SMARTS representations, a neural network model performs best ($R^2 \approx 0.82$–0.89), followed in performance by an RBF kernel support vector regressor ($R^2 \approx 0.73$–0.86), then random forest regression ($R^2$0.62–0.78), and finally linear ridge regression ($R^2 \approx 0.52$–0.67). A comparison of model results is displayed below in Tables 1 and 2. Training set metrics are in the supplementary information in Tables S1 and S2 and training curves are in the supplementary information in Fig. S1 and S2. Parity plots for all model predictions are available in the supplementary information in Fig. S5–S28.

We find that defining molecular structure by charge-resonance and ion functionalization according to the SMARTS representation we describe provides the best modeling results for room-temperature conductivity. These structural fragments better represent general ionic liquid conductivity trends in data-limited problems than the more detailed MACCS keys representation. This may indicate that ion core identities describe the broadest trends in ion mobility in ionic liquids which would

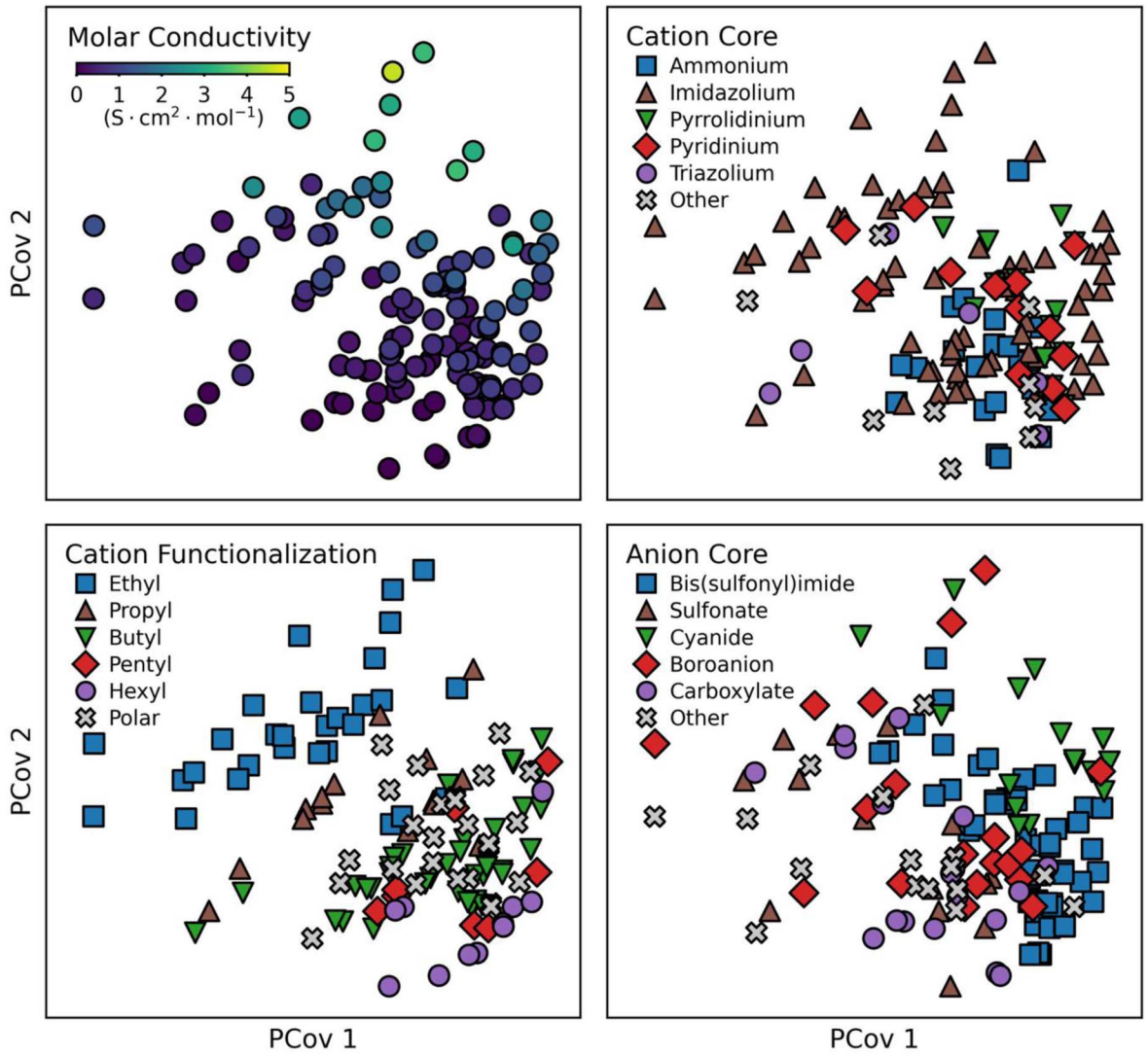

Fig. 5 2-Dimensional principal covariate data projections of 182 ionic liquids represented by our custom SMARTS fragmentation overlayed with molar conductivity at 298 K (Top Left), cation core identity (Top Right), cation functionalization (Bottom Left), and anion core identity (Bottom Right). Data clustering by cation functionalization and anion core identifies global correlations between structural similarity and molar conductivity.

agree with the consensus of the ionic liquid electrolyte community. Additional SMARTS representations can also be easily defined as additional data is collected to extend the fingerprint library while retaining interpretability. This provides ease of use for these models as a qualitative tool for ionic liquid design and screening.

We find that multilayer neural network models best predict ionic liquid conductivity using molecular fragment representations. The ability of neural networks to model ionic liquid conductivity from molecular structure agrees with contemporary studies.[12,14,27,28] In agreement with other machine learning studies for ionic liquids, the shortcomings of our model are indicative of the emergent nature of collective ionic liquid behavior which are not predictable from molecular details alone.[3,20,25,27] These emergent effects, such as nanostructuring, ionic correlations, and entropic effects, require experimental or simulation information to be considered.

Further analyzing our models, we find that prediction error increases while R^2 also increases when temperatures beyond 298 K are added to the dataset. Increasing the temperatures represented in our dataset increases the range of observed conductivities and adds more variations in our data for our regressions to model. While the positive correlation between temperature and conductivity is easily learned by all the regression techniques tested, the absolute error of predictions increases as relative errors scale with the predicted conductivity range. This indicates that changes to conductivity from temperature are not captured perfectly and compound upon the error of property–structure modeling. In fact, previous studies from our group and others indicate that temperature-conductivity scaling follows non-classical behavior.[12–14,82,95] This again iterates that ionic liquid conductivity is not easily described by temperature and structure, and advancements in machine learning modeling require additional novel information.

Conclusions

In this study we develop an ionic liquid SMARTS fragment data representation to improve the accuracy of regression models in low-data problems and identify structure–conductivity relationships. This new representation explicitly captures steric shielding and charge delocalization which is essential for modeling the dominant electrostatic interactions in ionic liquids. We further defined common ionic liquid functionalization to represent apolar, polar, and fluorine interactions within ionic liquids with reported experimental conductivity measurements. The final fragment representation identified 36 relevant ionic liquid structure fragments that we used in an RBF kernel regression to further analyze model weights and identify significant structure-conductivity trends.

We observe ionic liquid anion core identity and cation functionalization have more significant roles in determining ionic liquid conductivity than ionic liquid cation core identity. This is likely due to the greater variations in anion chemical structures and significant impacts of cation functionalization on ionic liquid nanostructure. Notably, we find that any substantial cation or anion functionalization (polar groups, 4C hydrocarbon tails, 2C fluorocarbon tails) decreases ion mobility as these functional groups can introduce additional intermolecular interactions and drive the formation of nanoscale segregation into ionic and non-ionic domains which likely increases energy penalties associated with fluid reorganization. Formation of nanoscale domains may be beneficial in ionic liquid mixtures, however, such as lithium and ionic liquids mixtures for example, where Li and ionic liquid cations are in competition for anion pairing and preferential mobilization of specific ionic species is desirable.

We further analyze our ionic liquid dataset by using PCovR to create a 2D projection of our data to find that PCov 2 captures a majority of the conductivity trend we unveil. The learned PCov weights are strong agreement with our RBF kernel regression, and our PCovR analysis identifies anion delocalization and cation alkyl functionalization as the dominant variations in ionic liquid molecular structures and the most deterministic structural motifs for ion conductivity. Analyzing the 2nd PCov, we identify structures which are structurally distinct yet have similarly low molar conductivity as well as common structural trends in the most conductive ionic liquids. We particularly identify weakly interacting cation functionalization and high-degrees of anion conformational flexibility, such as in as 1-ethyl-3-methylimidazolium dicyanamide, as an especially prevalent molecular motifs among the most conductive ionic liquids. This common motif may indicate similarities among these ionic liquids' nanostructure or transport mechanism and is an interesting point of further study.

Finally, we compare the accuracy of various regression methods and find that our fragment-based representation performs best for our low-data problem of predicting ionic liquid conductivity at 298 K. With only 182 ionic liquids and measurements, our SMARTS representation simplified model inputs for interpretable, shallow modeling. Overall, however, neural networks performed best for regressing conductivity at 298 K or all temperatures as these neural networks could better model the complex interactions in ionic liquid materials which contribute to ionic conductivity. In all models, however, we find persistent prediction errors that arise from an inability to represent proton transfer, steric effects, and conformational effects, and we conclude that additional material information will likely be needed to further improve conductivity prediction accuracies. In summary, we show how domain expertise in ionic liquids can be applied to data science techniques to improve data utilization and model insights in a data-limited investigation.

Methodology

Data processing

Experimentally reported absolute conductivities and densities were collected from ILThermo v2.0 for 182 ionic liquids.[36] As established in prior work,[12,13] molar conductivities are calculated by normalizing experimentally reported absolute conductivities by the ion concentration of the ionic liquid *via* the molecular weight and density as shown here:

$$\Lambda_{exp} = \frac{\lambda}{C} = \frac{\lambda \cdot M_w}{\rho}$$

where λ is absolute conductivity, C is concentration, M_w is molecular weight, ρ is density, and Λ_{exp} is the resulting molar conductivity. Absolute conductivities and densities are collected from the same study for each ionic liquid.

Ionic liquid fragmentation

We created one-hot encoded molecular fingerprints for each ionic liquid using SMARTS substructure matching to index the presence of molecular structure and their subsequent intermolecular interactions. Our SMARTS were defined to represent four major interaction types present in ionic liquids: electrostatic, non-polar, polar, and fluoroalkyl. Electrostatic SMARTS were defined by isolating the charge-carrying structures within the cationic and anionic species of the ionic liquids in our dataset. These were defined by the atoms and bonds that access the ions' formal charge *via* resonance. Symmetric resonance structures were not explicitly defined, as our SMARTS were not written to distinguish between stereoisomers.

Polar groups were defined as neutral functional groups containing oxygen or nitrogen. Non-polar groups were defined as neutral groups solely composed of carbon and hydrogen, including 5- and 6-membered aromatic rings and several aliphatic chain lengths. Fluorinated groups were defined as fluorocarbon aliphatic chains. These groups were defined separately from polar and nonpolar groups due to the significant differences in chemical and physical properties between fluorocarbon and hydrocarbon functional groups. The high frequency of anionic species that contain fluorine in our ionic liquid database further prompted us to define fluorinated groups separately. In particular, the formation of flouring-rich regimes in some ionic liquids is indicative of a separate, distinct phenomena.[68]

Ionic liquid featurization

Substructure matching was used to index SMARTS structures for each ionic liquid to create a matrix of ILs and SMARTS substructures. Each matrix column represents a specific SMARTS key, and each row represents an ionic liquid sample. A matrix element entry of 1 indicates the presence of a SMARTS structure in a specified ionic liquid for the respective column and row of the entry. 0 indicates the absence of the structure in the ionic liquid. An example visualization of the resulting matrix is available in the supplementary information in Fig. S4.

A matrix was created for all ionic liquids with molar conductivity at 298 K for our isothermal studies. Any substructure appearing fewer than 4 times or greater than 179 times for our 182 ionic liquids were removed during regressions to reduce overfitting and simplify our analysis. Matrices were prepared for the cationic and anionic SMARTS keys separately before being concatenated together to form a final binary matrix for a given dataset of ionic liquids, which was used for training and testing machine learning models. For temperature-dependent analyses, the temperature of each ionic liquid in the database was concatenated into the final column of the existing bit matrix for additional analysis, ranging from 273 K to 373 K, and additional ionic liquids, missing property reporting at 298 K, were added to the dataset.

Conductivity regressions

Ionic liquid molar conductivity was regressed using linear support vector machines, radial basis function kernel support vector machines, random forests, and neural networks *via* Sci-Kit Learn libraries. We implemented 10-fold cross validation to report model performance and conduct hyperparameter tuning. During 10-fold cross validation, the dataset was split into 10 random sets according to the ionic liquid compound names to ensure the same ionic liquid at varied temperatures does not appear in both the training and test set for a given split. This provided a prediction value for each data point in the presented regression plots, and values reported here are for the test set performances. Training set performances can be found in the supplementary information.

Support vector machine regressions were created to model ionic liquid conductivity using our ionic liquid molecular fingerprints and investigate global substructure contributions to conductivity. RBF kernel regression weights were analyzed to determine the group's contributions to ionic liquid transport properties when allowing for local fitting. We extract individual substructure weights from the RBF kernel regression by predicting the conductivity of a vector with only a single substructure descriptor for each substructure defined.

Random forest and neural network regression models were created using the sci-kit learn library for comparison to the linear regression models. Hyperparameters for these models were tuned to minimize 10-fold cross validated mean squared error (MSE). A random forest was used to investigate the fit of logic-based decision trees on our one-hot encoded molecular representation and determine the continuity of contributions to conductivity from molecular motifs. We used a multilayer perceptron (MLP) artificial neural network to capture nonlinear interactions between the defined intramolecular ionic liquid functional groups and observe the effects of increased model complexity.

Model evaluation

Root Mean Squared (RMSE)

$$RMSE = \sqrt{\frac{1}{n}\sum_{i}^{n}\left(P_i - P_{predicted,i}\right)^2}$$

and Error and coefficient of determination (R^2)

$$R^2 = 1 - \frac{\sum_i \left(P_i - P_{predicted,i}\right)^2}{\sum_i \left(P_i - \frac{1}{n}\sum_i^n P_i\right)^2}$$

were used to evaluate model performance. P_i is the target value, $P_{predicted,i}$ is the model prediction, and n is the total number of data points.

Dimensionality reduction

Principal Covariates Regression is utilized using Sci-Kit Matter[91] to identify prominent ionic liquid profiles which are most informative for ionic liquid conductivity regressions. Ionic liquid conductivity is regressed using our one-hot encoded molecular representation while our data's dimensionality is simultaneously reduced by 2-dimensional principal components analysis to best model conductivity.[92,93] The resulting principal covariates are analyzed to identify the most significant ionic liquid molecular fragment profiles for conductivity modeling.

Author contributions

Research was conceptualized by M. A. G., V. M. Z., R. K. C., and J. E. U. Data was curated by J. E. U. and N. A. Z. Formal Analysis was performed by J. E. U. and N. A. Z. Funding was acquired by M. A. G. and V. M. Z. Investigations were performed by J. E. U. and N. A. Z. Computational studies were performed by J. E. U. and N. A. Z. Data was analyzed by M. A. G., V. M. Z., R. K. C., and J. E. U. Methodology was developed by J. E. U. and N. A. Z. Project Administration by M. A. G., V. M. Z., and R. K. C. Software was developed by J. E. U. and N. A. Z. Resources were provided by M. A. G. and V. M. Z. Research was supervised by M. A. G., V. M. Z., and R. K. C. Result validation was performed by J. E. U. Visualizations were created by M. A. G., V. M. Z., R. K. C., J. E. U, and N. A. Z. Written by M. A. G., V. M. Z., R. K. C., J. E. U, and N. A. Z. Reviewed and Edited by M. A. G., V. M. Z., R. K. C., and J. E. U.

Conflicts of interest

There are no conflicts to declare.

Data availability

All data and code needed to reproduce the analysis is available in the GitHub repository https://github.com/zavalab/ML/tree/master/IonicLiquids_SMARTS and is published on Zenodo at https://doi.org/10.5281/zenodo.19009489.

Supplementary information (SI) is available. See DOI: https://doi.org/10.1039/d6sc02121b.

Acknowledgements

Support for this research was primarily provided by the University of Wisconsin–Madison Office of the Vice Chancellor for Research *via* the Wisconsin Alumni Research Foundation, the National Science Foundation Graduate Research Fellowship Program under Grant No. DGE-2137424, and the National Science Foundation Division of Materials Research under Grant No. DMR-2309000. Any opinions, findings, and conclusions or recommendations expressed in this material are those of the author(s) and do not necessarily reflect the views of the National Science Foundation. Additional sponsorship for research was provided by the Army Research Laboratory and was accomplished under Grant Number W911NF-26-1-A040. The views and conclusions contained in this document are those of the authors and should not be interested as representing the offficial policies, either expressed or implied, of the Army Research Laboratory or the U.S. Government. The U.S. Government is authorized to reproduce and distribute reprints for Government purposes notwithstanding any copyright notation herein.

References

1 P. Nancarrow, A. Al-Othman, D. K. Mital and S. Dopking, *Energy*, 2021, 220.
2 F. Philippi, D. Pugh, D. Rauber, T. Welton and P. A. Hunt, *Chem. Sci.*, 2020, **11**, 6405–6422.
3 F. Philippi and T. Welton, *Phys. Chem. Chem. Phys.*, 2021, **23**, 6993–7021.
4 Z. Song, J. Chen, J. Cheng, G. Chen and Z. Qi, *Chem. Rev.*, 2024, **124**, 248–317.
5 T. Welton, *Biophys. Rev.*, 2018, **10**, 691–706.
6 C. Zhong, Y. Deng, W. Hu, J. Qiao, L. Zhang and J. Zhang, *Chem. Soc. Rev.*, 2015, **44**, 7484–7539.
7 X. Mao, P. Brown, C. Červinka, G. Hazell, H. Li, Y. Ren, D. Chen, R. Atkin, J. Eastoe, I. Grillo, A. A. H. Padua, M. F. Costa Gomes and T. A. Hatton, *Nat. Mater.*, 2019, **18**, 1350–1357.
8 J. M. Klein, E. Panichi and B. Gurkan, *Phys. Chem. Chem. Phys.*, 2019, **21**, 3712–3720.
9 S. Koutsoukos, F. Philippi, F. Malaret and T. Welton, *Chem. Sci.*, 2021, **12**, 6820–6843.
10 N. V. Plechkova and K. R. Seddon, *Chem. Soc. Rev.*, 2008, **37**, 123–150.
11 F. Philippi, D. Rauber, K. L. Eliasen, N. Bouscharain, K. Niss, C. W. M. Kay and T. Welton, *Chem. Sci.*, 2022, **13**, 2735–2743.
12 J. E. Umaña, R. K. Cashen, V. M. Zavala and M. A. Gebbie, *Digital Discovery*, 2025, **4**, 1423–1436.
13 R. K. Cashen, M. M. Donoghue, A. J. Schmeiser and M. A. Gebbie, *J. Phys. Chem. B*, 2022, **126**, 6039–6051.
14 I. Baskin, A. Epshtein and Y. Ein-Eli, *J. Mol. Liq.*, 2022, **351**, 118616.
15 W. D. Amith, J. C. Araque and C. J. Margulis, *J. Ionic Liquid.*, 2022, **2**, 100012.
16 S. I. Lall-Ramnarine, M. Zhao, C. Rodriguez, R. Fernandez, N. Zmich, E. D. Fernandez, S. B. Dhiman, E. W. Castner and J. F. Wishart, *J. Electrochem. Soc.*, 2017, **164**, H5247.
17 M. A. Zebida, K. Argoub, A. M. Benkouider, A. Yahiaoui, K. Toubal and A. Hachemaoui, *Fluid Phase Equilib.*, 2024, **579**, 114024.
18 R. Datta, R. Ramprasad and S. Venkatram, *J. Chem. Phys.*, 2022, **156**, 214505.
19 T. E. Karakasidis, F. Sofos and C. Tsonos, *Fluids*, 2022, **7**, 321.
20 Z. Chen, J. Chen, Y. Qiu, J. Cheng, L. Chen, Z. Qi and Z. Song, *ACS Sustain. Chem. Eng.*, 2024, **12**, 6648–6658.
21 R. Nakhaei-Kohani, S. Ali Madani, S.-P. Mousavi, S. Atashrouz, A. Abedi, A. Hemmati-Sarapardeh and A. Mohaddespour, *J. Mol. Liq.*, 2022, **362**, 119509.

22 C. Song, C. Wang, F. Fang, G. Zhou, Z. Dai and Z. Yang, *J. Chem. Eng. Data*, 2024, **69**, 4310–4319.
23 Z. K. Koi, W. Z. N. Yahya and K. A. Kurnia, *New J. Chem.*, 2021, **45**, 18584–18597.
24 M. Abdullah, K. Chellappan Lethesh, A. A. B. Baloch and M. O. Bamgbopa, *J. Mol. Liq.*, 2022, **368**, 120620.
25 M. Mohan, K. D. Jetti, S. Guggilam, M. D. Smith, M. K. Kidder and J. C. Smith, *ACS Sustain. Chem. Eng.*, 2024, **12**, 7040–7054.
26 C. Wang, C. Song, G. Zhou, Z. Dai and Z. Yang, *J. Chem. Eng. Data*, 2024, **69**, 4350–4361.
27 A. Seshadri, L. T. M. Hess and S. Yue, *Digital Discovery*, 2026, **5**, 1709–1717.
28 P. Dhakal and J. K. Shah, *Mol. Syst Des. Eng.*, 2022, **7**, 1344–1353.
29 N. Molinari, J. P. Mailoa, N. Craig, J. Christensen and B. Kozinsky, *J. Power Sources*, 2019, **428**, 27–36.
30 F. Philippi, D. Rauber, J. Zapp, C. Prasang, D. Scheschkewitz and R. Hempelmann, *Chemphyschem*, 2019, **20**, 443–455.
31 L. K. Scarbath-Evers, P. A. Hunt, B. Kirchner, D. R. MacFarlane and S. Zahn, *Phys. Chem. Chem. Phys.*, 2015, **17**, 20205–20216.
32 J. C. Araque, J. J. Hettige and C. J. Margulis, *J. Phys. Chem. B*, 2015, **119**, 12727–12740.
33 L. Caradant, N. Verdier, G. Foran, D. Lepage, A. Prebe, D. Ayme-Perrot and M. Dolle, *ACS Appl. Polym. Mater.*, 2021, **3**, 6694–6704.
34 J. Vila, P. Ginés, J. M. Pico, C. Franjo, E. Jiménez, L. M. Varela and O. Cabeza, *Fluid Phase Equilib.*, 2006, **242**, 141–146.
35 M. Videa and C. A. Angell, *J. Phys. Chem. B*, 1999, **103**, 4185–4190.
36 A. F. Kazakov, J. W. Magee, R. D. Chirico, V. Diky, K. G. Kroenlein, C. D. Muzny and M. D. Frenkel, *Ionic Liquids Database - ILThermo (v2.0)*, 2013.
37 D. Qian, M. Chris, K. Andrei, D. Vladimir, M. Joe, W. Jason, C. Robert, M. Kenneth and F. Michael, *J. Chem. Eng. Data*, 2007, **52**(4), 1151–1159.
38 A. Mariani, M. Bonomo, X. Gao, B. Centrella, A. Nucara, R. Buscaino, A. Barge, N. Barbero, L. Gontrani and S. Passerini, *J. Mol. Liq.*, 2021, **324**, 115069.
39 K. R. Harris, *J. Phys. Chem. B*, 2019, **123**, 7014–7023.
40 J. L. Durant, B. A. Leland, D. R. Henry and J. G. Nourse, *J. Chem. Inf. Comput. Sci.*, 2002, **42**, 1273–1280.
41 *RDKit: Open-Source Cheminformatics Software*, https://www.rdkit.org/, accessed 8/8/2022, 2022.
42 SMARTS: A Language for Describing Molecular Patterns, http://www.daylight.com/dayhtml/doc/theory/theory.smarts.html.
43 R. K. Cersonsky, M. Pakhnova, E. A. Engel and M. Ceriotti, *Chem. Sci.*, 2023, **14**, 1272–1285.
44 J. C. Araque, S. K. Yadav, M. Shadeck, M. Maroncelli and C. J. Margulis, *J. Phys. Chem. B*, 2015, **119**, 7015–7029.
45 K. D. Fong, J. Self, B. D. McCloskey and K. A. Persson, *Macromolecules*, 2021, **54**, 2575–2591.
46 R. Ogbodo, W. V. Karunaratne, G. R. Acharya, M. S. Emerson, M. Mughal, H. M. Yuen, N. Zmich, S. Nembhard, F. Wang, H. Shirota, S. I. Lall-Ramnarine, E. W. Castner, Jr., J. F. Wishart, A. J. Nieuwkoop and C. J. Margulis, *J. Phys. Chem. B*, 2023, **127**, 6342–6353.
47 T. L. Greaves and C. J. Drummond, *Chem. Rev.*, 2015, **115**, 11379–11448.
48 D.-J. Tao, Z. Cheng, F.-F. Chen, Z.-M. Li, N. Hu and X.-S. Chen, *J. Chem. Eng. Data*, 2013, **58**, 1542–1548.
49 Z. Wojnarowska, Y. Wang, J. Pionteck, K. Grzybowska, A. P. Sokolov and M. Paluch, *Phys. Rev. Lett.*, 2013, **111**, 225703.
50 K. B. Dhungana, L. F. O. Faria, B. Wu, M. Liang, M. C. C. Ribeiro, C. J. Margulis and E. W. Castner, Jr., *J. Chem. Phys.*, 2016, **145**(2), 024503.
51 H. Weber and B. Kirchner, *J. Phys. Chem. B*, 2016, **120**, 2471–2483.
52 F. Philippi, D. Rauber, O. Palumbo, K. Goloviznina, J. McDaniel, D. Pugh, S. Suarez, C. C. Fraenza, A. Padua, C. W. M. Kay and T. Welton, *Chem. Sci.*, 2022, **13**, 9176–9190.
53 T. Pranto, C. C. Fraenza, F. Philippi, D. Rauber, C. W. M. Kay, T. Welton, S. G. Greenbaum and S. Suarez, *Phys. Chem. Chem. Phys.*, 2025, **27**, 2462–2472.
54 H. Zhang, X. Cheng, Q. Ma, W. Feng, L. Zheng, J. Nie, X. Huang, M. Armand and Z. Zhou, *Electrochim. Acta*, 2016, **207**, 66–75.
55 P. A. Hunt, I. R. Gould and B. Kirchner, *Aust. J. Chem.*, 2007, **60**, 9–14.
56 S. Tsuzuki, H. Tokuda, K. Hayamizu and M. Watanabe, *J. Phys. Chem. B*, 2005, **109**, 16474–16481.
57 S. N. Suarez, A. Rúa, D. Cuffari, K. Pilar, J. L. Hatcher, S. Ramati and J. F. Wishart, *J. Phys. Chem. B*, 2015, **119**, 14756–14765.
58 S. Seki, T. Kobayashi, Y. Kobayashi, K. Takei, H. Miyashiro, K. Hayamizu, S. Tsuzuki, T. Mitsugi and Y. Umebayashi, *J. Mol. Liq.*, 2010, **152**, 9–13.
59 S. A. Forsyth, J. M. Pringle and D. R. MacFarlane, *Aust. J. Chem.*, 2004, **57**, 113–119.
60 E. I. Izgorodina, M. Forsyth and D. R. MacFarlane, *Aust. J. Chem.*, 2007, **60**, 15–20.
61 A. S. M. C. Rodrigues, C. F. R. A. C. Lima, J. A. P. Coutinho and L. M. N. B. F. Santos, *Phys. Chem. Chem. Phys.*, 2017, **19**, 5326–5332.
62 P. Bonhôte, A.-P. Dias, N. Papageorgiou, K. Kalyanasundaram and M. Grätzel, *Inorg. Chem.*, 1996, **35**, 1168–1178.
63 I. Bandrés, D. F. Montaño, I. Gascón, P. Cea and C. Lafuente, *Electrochim. Acta*, 2010, **55**, 2252–2257.
64 Y. Zhang and E. J. Maginn, *Phys. Chem. Chem. Phys.*, 2012, **14**, 12157–12164.
65 U. G. Brauer, A. T. De La Hoz and K. M. Miller, *J. Mol. Liq.*, 2015, **210**, 286–292.
66 A. T. De La Hoz, U. G. Brauer and K. M. Miller, *J. Phys. Chem. B*, 2014, **118**, 9944–9951.
67 Z. K. Reeder, A. M. Adler and K. M. Miller, *Tetrahedron Lett.*, 2016, **57**, 206–209.
68 M. Brehm, H. Weber, M. Thomas, O. Hollóczki and B. Kirchner, *Chemphyschem*, 2015, **16**, 3271–3277.
69 J. N. A. Canongia Lopes and A. A. H. Pádua, *J. Phys. Chem. B*, 2006, **110**, 3330–3335.

70 Y. Wang and G. A. Voth, *J. Phys. Chem. B*, 2006, **110**, 18601–18608.
71 R. Hayes, G. G. Warr and R. Atkin, *Chem. Rev.*, 2015, **115**, 6357–6426.
72 S. M. Urahata and M. C. C. Ribeiro, *J. Chem. Phys.*, 2004, **120**, 1855–1863.
73 M. B. Herath, T. Hickman, S. E. Creager and D. D. DesMarteau, *J. Fluorine Chem.*, 2011, **132**, 52–56.
74 M. Zhao, B. Wu, S. I. Lall-Ramnarine, J. D. Ramdihal, K. A. Papacostas, E. D. Fernandez, R. A. Sumner, C. J. Margulis, J. F. Wishart and E. W. Castner, Jr., *J. Chem. Phys.*, 2019, **151**(7), 074504.
75 C. S. M. Kang, X. Zhang and D. R. MacFarlane, *J. Phys. Chem. C*, 2018, **122**, 24550–24558.
76 D. Rauber, F. Philippi, B. Kuttich, J. Becker, T. Kraus, P. Hunt, T. Welton, R. Hempelmann and C. W. M. Kay, *Phys. Chem. Chem. Phys.*, 2021, **23**, 21042–21064.
77 A. Paul and A. Samanta, *J. Phys. Chem. B*, 2007, **111**, 4724–4731.
78 Z. Chen, Y. Huo, J. Cao, L. Xu and S. Zhang, *Ind. Eng. Chem. Res.*, 2016, **55**, 11589–11596.
79 M. Kanakubo, K. R. Harris, N. Tsuchihashi, K. Ibuki and M. Ueno, *J. Chem. Eng. Data*, 2015, **60**, 1495–1503.
80 K. Yoshii, T. Uto, T. Onishi, D. Kosuga, N. Tachikawa and Y. Katayama, *Chemphyschem*, 2021, **22**, 1584–1594.
81 T. Makino, M. Kanakubo, Y. Masuda, T. Umecky and A. Suzuki, *Fluid Phase Equilib.*, 2014, **362**, 300–306.
82 P. Nürnberg, J. Atik, O. Borodin, M. Winter, E. Paillard and M. Schönhoff, *J. Am. Chem. Soc.*, 2022, **144**, 4657–4666.
83 V. Delhorbe, D. Bresser, H. Mendil-Jakani, P. Rannou, L. Bernard, T. Gutel, S. Lyonnard and L. Picard, *Macromolecules*, 2017, **50**, 4309–4321.
84 S. Jana, A. Parthiban and C. L. L. Chai, *Chem. Commun.*, 2010, **46**, 1488–1490.
85 D. Penley, X. Y. Wang, Y. Y. Lee, M. N. Garaga, R. Ghahremani, S. Greenbaum, E. J. Maginn and B. Gurkan, *J. Chem. Eng. Data*, 2022, **67**, 1810–1823.
86 J. McAlpine, M. Rebarchik, H. Tupkar, Z. Jiang, S. Alemdar, M. Gallmeyer, J. E. Dahl, R. M. K. Carlson, B. O. Tkachenko, H. Hofstetter, C. F. M. Clewett, P. R. Schreiner, W. S. Loo, M. Mavrikakis and M. A. Gebbie, *J. Mater. Chem. A*, 2025, **13**, 36341–36350.
87 J. McAlpine, A. Bloemendal, J. E. Dahl, R. M. K. Carlson, I. A. Guzei, C. F. M. Clewett, B. O. Tkachenko, P. R. Schreiner and M. A. Gebbie, *Chem. Mater.*, 2023, **35**, 3545–3554.
88 M. Forsyth, H. Yoon, F. Chen, H. Zhu, D. R. MacFarlane, M. Armand and P. C. Howlett, *J. Phys. Chem. C*, 2016, **120**, 4276–4286.
89 Q. Huang, T. C. Lourenço, L. T. Costa, Y. Zhang, E. J. Maginn and B. Gurkan, *J. Phys. Chem. B*, 2019, **123**, 516–527.
90 J. B. Haskins, W. R. Bennett, J. J. Wu, D. M. Hernández, O. Borodin, J. D. Monk, C. W. Bauschlicher, Jr. and J. W. Lawson, *J. Phys. Chem. B*, 2014, **118**, 11295–11309.
91 A. Goscinski, V. Principe, G. Fraux, S. Kliavinek, B. Helfrecht, P. Loche, M. Ceriotti and R. Cersonsky, *Open Res. Eur.*, 2023, **3**, 81.
92 R. K. Cersonsky, B. A. Helfrecht, E. A. Engel, S. Kliavinek and M. Ceriotti, *Mach. Learn.: Sci. Technol.*, 2021, **2**, 035038.
93 B. A. Helfrecht, R. K. Cersonsky, G. Fraux and M. Ceriotti, *Mach. Learn.: Sci. Technol.*, 2020, **1**(4), 045021.
94 J. M. Pringle, J. Golding, K. Baranyai, C. M. Forsyth, G. B. Deacon, J. L. Scott and D. R. MacFarlane, *New J. Chem.*, 2003, **27**, 1504–1510.
95 H. K. Kashyap, H. V. R. Annapureddy, F. O. Raineri and C. J. Margulis, *J. Phys. Chem. B*, 2011, **115**, 13212–13221.